

Journal Pre-proof

Nano adamantane-conjugated BODIPY for lipase affinity and light driven antibacterial

Jian Shao, Pu-Zhen Huang, Qiu-Yun Chen, Qing-Lin Zheng



PII: S1386-1425(20)30230-4

DOI: <https://doi.org/10.1016/j.saa.2020.118252>

Reference: SAA 118252

To appear in: *Spectrochimica Acta Part A: Molecular and Biomolecular Spectroscopy*

Received date: 17 February 2020

Revised date: 7 March 2020

Accepted date: 10 March 2020

Please cite this article as: J. Shao, P.-Z. Huang, Q.-Y. Chen, et al., Nano adamantane-conjugated BODIPY for lipase affinity and light driven antibacterial, *Spectrochimica Acta Part A: Molecular and Biomolecular Spectroscopy* (2020), <https://doi.org/10.1016/j.saa.2020.118252>

This is a PDF file of an article that has undergone enhancements after acceptance, such as the addition of a cover page and metadata, and formatting for readability, but it is not yet the definitive version of record. This version will undergo additional copyediting, typesetting and review before it is published in its final form, but we are providing this version to give early visibility of the article. Please note that, during the production process, errors may be discovered which could affect the content, and all legal disclaimers that apply to the journal pertain.

© 2020 Published by Elsevier.

Nano adamantane-conjugated BODIPY for lipase affinity and light driven antibacterialJian Shao^a, Pu-Zhen Huang^a, Qiu-Yun Chen^{*a}, Qing-Lin Zheng^{a,b}^aSchool of Chemistry and Chemical Engineering, Jiangsu University, Zhenjiang, 212013, China.^bTHOR Specialty Chemical (Zhenjiang) Company Limited, No. 182 Jingang Avenue, New District, Zhenjiang, Jiangsu, 212132, China.* Corresponding Author, E-mail: chengy@ujs.edu.cn.**ABSTRACT**

The increasing number of resistant bacterial strains has raised efforts in developing alternative treatment strategies. Lipase is highly expressed in most bacteria and lipase targeting dyes will be non-sacrificed materials for a sustainable method against microorganism. The combination of chemotherapy and antimicrobial photodynamic inactivation (aPDI) method will be an effective method due to enhanced antibacterial activity. Here we reported the spectroscopic features of five boron dipyrrolylmethene (BODIPY) derivatives with different functional groups for lipase affinity and antibacterial activity. Lipase affinity tests and antibacterial assays were conducted by spectroscopic methods. Adamantane-conjugated BODIPY (BDP-2) was found to be the active compound against *E. coli*. Next, BDP-2 was brominated, and then assembled with PEG resulting biocompatible BDP2-Br₂@mPEG nanoparticles. The MTT assay indicated that BDP2-Br₂@mPEG was less toxicity on BGC-823 cancer cells without irradiation. The BDP2-Br₂@mPEG can inhibit the proliferation of *E. coli* and damage the membrane of bacterial cell under green LED light irradiation. The results proved BDP2-Br₂@mPEG can be a very promising green LED light driven antibacterial material.

Keywords: BODIPY, adamantane, antibacterial, photodynamic therapy, single oxygen

1. Introduction

The severity of bacterial infectious diseases has caused worldwide concern. The abuse of antibiotics has caused bacterial resistance mutations, making people commit to find more suitable antibacterial methods [1-3]. Antimicrobial photodynamic inactivation (aPDI) has been introduced into bacteriostatic treatment [3-4]. The aPDI utilizes a photosensitizer (PS) to produce reactive oxygen species (ROS) including singlet oxygen ($^1\text{O}_2$) or free radicals when PS is illuminated with visible or near-infrared light. Singlet oxygen can destruct bacterial reactivity with most biomolecules, and it can be turned into harmless oxygen [5-8]. More importantly, due to non-specific damage caused by $^1\text{O}_2$, its killing effect does not cause any drug resistance of pathogenic bacteria [9].

Boron dipyrrolylmethene (BODIPY) is a kind of tunable fluorescent dyes for photodynamic therapy (PDT) and aPDI [10]. Functional groups conjugated BODIPY derivatives can convert the O_2 into singlet oxygen ($^1\text{O}_2$) against cancer cells or bacteria under irradiation [11-14]. Specific structures in BODIPY derivatives can also increase the bacteria targeting affinity [15]. Nitazoxanide and benzamide derivatives were found to be useful class of functional groups in those reported antibacterial agents [16-17]. Moreover, adamantane derivatives can interfere with a variety of enzymes, and have good therapeutic activities such as anti-viral, anti-Parkinson, antibacterial and anti-cancer [18-19]. Therefore, multifunctional photodynamic therapy may have the advantages of both photodynamic therapy and chemotherapy. BODIPYs are recently studied in biological areas because of its good absorption to visible light. Lipases are the components of the outer membrane of Gram-negative bacteria. Compounds with aromatic amides groups, such as 1,2,3-triazole ureas and 1,5-diphenylpyrazole-3-carboxamide derivatives were as selective lipase inhibitors

[20, 21]. Therefore, the conjugates of functional groups (such as benzamide, adamantane, etc.) with BODIPY would have the potential properties of both lipase recognition and visible light-driven photodynamic inactivation. Over-dose antibacterial agents have been demonstrated to be harmful for both environments and human being. The lipase targeting PDT agent could be an effective and green antibacterial agent due to its selectivity and visible light-driven photodynamic inactivation, which would have a smaller impact on normal lives.

In this work, we conceived a design that employed BODIPY part as a photosensitizer, bromine as heavy atom to generate singlet oxygen, and functional groups (such as benzamide, adamantane, etc.) as lipase targeting and anti-bacterial functional group (Scheme 1). To enhance the biocompatible property of dyes, a nano-dye (BDP2-Br₂@mPEG) was produced. Porcine pancreatic lipase (PL) was used to screen the affinity of compounds with lipase. Activities against *E. coli* were studied with and without illumination.

2. Materials and Methods

2.1 Reagents

All chemicals were purchased from commercial suppliers and were used without further purification. 2, 4-Dimethylpyrrole (98%), *p*-chloromethylbenzoyl chloride, adamantane, methyl bromoacetate and N-bromosuccinimide (NBS), 1,2-distearoyl-sn-glycero-3-phosphoethanolamine-N-[methoxy(polyethyleneglycol)-5000] (DSPE-mPEG5000) and other chemicals were purchased from Energy Chemical Reagent Co., Ltd. LB broth and agar were purchased from Sangon Biotech (Shanghai, China) Co., Ltd. The bacterial strain *Escherichia coli* (*E. coli*, ATCC 25922) were obtained from Luwei Technology (Shanghai, China) Co., Ltd. (3s,5s,7s)-N-(4-(5,5-difluoro-1,3,7,9-tetramethyl-5H-4λ⁴,5λ⁴-dipyrrolo[1,2-c:2',1'-f][1,3,2]diazaborin-10-yl)benzyl)adamantan-1-amine (BDP-Ad) and 8-(4-chlorobenzyl)-4,4-difluoro-1,3,5,7-

tetramethyl-4-bora-3a,4a-diaza-sindacen (BODIPY-Cl) were synthesized according to literature procedures [22, 23].

2.2 Characterization

The electronic absorption spectra were measured at room temperature by a UV-2450 UV-vis spectrophotometer. Fluorescence measurements were carried out on a fluorescence spectrofluorometer Model CARY Eclipse (VARIAN, USA), a 1.0 cm quartz cell (slit width = 5 nm). The ^1H NMR (400 MHz) and ^{13}C NMR (100 MHz) data was recorded on a Bruker AVANCE II 400 MHz spectrometer using CDCl_3 as a solvent. The chemical shifts (δ) were reported in ppm and coupling constants (J) in Hz. The electrospray mass spectra (ES-MS) were measured on a Finnigan LCQ mass spectrograph. The fluorescence lifetime was determined using a time-dependent single photon counting setup (TCSPC) (Fluo Time 200, Picoquant GmbH). The size distribution of the nanoparticle was measured on a Brookhaven BI-9000 (Brookhaven Instruments, US). The SEM images of the samples were obtained by using a scanning electron microscope (SEM, Shimadzu SS-550).

2.3 Synthesis of 1-(4-(5,5-difluoro-1,3,7,9-tetramethyl-5H-4 λ^4 ,5 λ^4 -dipyrrolo [1,2-c:2',1'-f][1,3,2]diazaborin-10-yl)benzyl)-N-(5-nitrothiazol-2-yl)pyrrolidine-2-carboxamide (BDP-1)

BODIPY-Cl (500 mg, 1.34 mmol) and L-proline (154 mg, 1.34 mmol) were dissolved in THF (20 mL) at room temperature. After mixing evenly, Et_3N (186 μL , 1.34 mmol), KI (80 mg, 0.48 mmol) and three drops of 18-crown-6 were added. After the reaction mixture was heated to 65 $^\circ\text{C}$ in an oil bath and stirred for 10 h, the solution was concentrated and recrystallized with ethyl acetate to get the crude intermediate. The final product was synthesized according to literature procedures with slight modification [24]. The crude intermediate (540 mg, 1.2 mmol) was dissolved in DCM (10 mL), 2-amino-5-nitro-thiazol (173 mg, 1.2 mmol), DCC (375 mg, 1.8 mmol) and DMAP (61 mg, 0.5

mmol) were then added under N₂ atmosphere. The reaction mixture was stirred at room temperature overnight. The solvent was removed *in vacuo* and residue was dissolved in DCM. The organic layer was washed with saturated sodium chloride (3×10 mL), dried with sodium sulfate, and concentrated *in vacuo*. The residue was loaded onto a column of silica gel to give BDP-1 (245 mg, 42% yield) as an orange solid. ¹H NMR (400 MHz, CDCl₃) δ 8.34 (s, 1H), 7.49 (d, *J* = 7.8 Hz, 2H), 7.30 (d, *J* = 9.0 Hz, 2H), 5.98 (s, 2H), 3.91 (dd, *J* = 9.6, 12.6 Hz, 2H), 3.21 (t, *J* = 7.4 Hz, 1H), 2.65 (d, *J* = 5.8 Hz, 1H), 2.56 (s, 6H), 2.47 – 2.28 (m, 1H), 2.14 – 1.70 (m, 4H), 1.30 (s, 6H). ¹³C NMR (100 MHz, CDCl₃) δ 160.30, 155.69, 143.69, 142.79, 140.77, 134.83, 131.32, 129.91, 128.62, 121.36, 65.89, 59.93, 54.51, 31.44, 31.00, 30.20, 29.69, 24.55, 14.57, 14.32. ES-MS(ESI, MeOH): Calcd for C₂₈H₂₉BF₂N₆O₃S [M-H]⁻ *m/z*=577.45, found *m/z*=577.31.

2.4 Synthesis of methyl N-((3s,5s,7s)-adamantan-1-yl)-N-(4-(5,5-difluoro-1,3,7,9-tetramethyl-5H-4λ⁴,5λ⁴-dipyrrolo[1,2-c:2',1'-f][1,3,2]diazaborinin-10-yl)benzyl)glycinate (BDP-2)

BODIPY-Ad (487 mg, 1 mmol) was dissolved in MeCN (20 mL) at room temperature, then methyl bromoacetate (306 mg, 2 mmol) and Et₃N (202 mg, 2 mmol) were added. After the reaction mixture was heated to 80 °C in an oil bath and stirred for 10 h, orange solution was obtained. The solvent was removed *in vacuo* and residue was dissolved in DCM. The organic layer was washed with saturated sodium chloride (3×10 mL), dried with sodium sulfate, and then concentrated *in vacuo*. The residue was loaded onto a column of silica gel to give BDP-2 (352 mg, 63% yield) as an orange solid. ¹H NMR (400 MHz, CDCl₃) δ: 7.56 (d, *J* = 8.0 Hz, 2H), 7.21 (d, *J* = 8.0 Hz, 2H), 5.98 (s, 2H), 4.00 (s, 2H), 3.64 (s, 3H), 3.39 (s, 2H), 2.57 (s, 6H), 2.12 (s, 3H), 1.81 (d, *J* = 2.1 Hz, 6H), 1.66 (q, *J* = 12.2 Hz, 6H), 1.39 (s, 6H). ¹³C NMR (100 MHz, CDCl₃) δ: 174.03, 155.22, 143.13, 142.19, 133.14, 131.56, 129.27, 127.62, 121.10, 55.19, 51.34, 51.20, 48.93, 40.15, 36.63, 29.73,

14.55, 14.32. ES-MS (ESI⁺, CH₃CN): Calcd for C₃₃H₄₀BF₂N₃O₂ [M+H]⁺ m/z=560.51, found m/z=560.96.

2.5 Synthesis of methyl N-((3s,5s,7s)-adamantan-1-yl)-N-(4-(2,8-dibromo-5,5-difluoro-1,3,7,9-tetramethyl-5H-4λ⁴,5λ⁴-dipyrrolo[1,2-c:2',1'-f][1,3,2]diazaborinin-10-yl)benzyl)glycinate (BDP2-Br₂)

BDP-2 (280 mg, 0.5 mmol) and NBS (334 mg, 2 mmol) were dissolved in dry CH₂Cl₂ (20 mL) at room temperature. After stirred at room temperature for 30 min, the solvent was removed *in vacuo*. The residue was loaded onto a column of silica gel to give BDP2-Br₂ (308 mg, 86% yield) as a red solid. ¹H NMR (400 MHz, CDCl₃) δ: 7.61 (d, *J* = 7.9 Hz, 2H), 7.17 (d, *J* = 8.0 Hz, 2H), 4.01 (s, 2H), 3.65 (s, 3H), 3.40 (s, 2H), 2.61 (s, 6H), 2.12 (s, 3H), 1.80 (s, 6H), 1.66 (q, *J* = 12.2 Hz, 6H), 1.38 (s, 6H). ¹³C NMR (100 MHz, CDCl₃) δ: 173.90, 153.70, 143.77, 142.63, 140.62, 132.46, 130.53, 129.53, 127.43, 111.67, 111.64, 55.32, 51.40, 51.30, 49.05, 40.14, 36.62, 29.72, 13.66. ES-MS (ESI⁺, CH₃CN): Calcd for C₃₃H₃₈BBr₂F₂N₃O₂ [M+H]⁺ m/z=718.30, found m/z=718.47.

2.6 General Procedure for the Synthesis of Benzoyl Piperazine BODIPYs

Benzoic acid (366 mg, 3 mmol), 1-boc-piperazine (560 mg, 3 mmol), DCC (927 mg, 4.5 mmol) and DMAP (122 mg, 1 mmol) were dissolved in DCM (10 mL) at room temperature under N₂ atmosphere. The reaction mixture was stirred for 10 h before it was filtered. The mixture solution was then concentrated *in vacuo* and the residue was loaded onto a column of silica gel to give crude piperazine benzoic acylamide as a white solid. Piperazine benzoic acylamide (830 mg, 2.8 mmol) was dissolved in DCM (5 mL) and TFA (1 mL) was added. The reaction mixture was stirred for 10 h before it was concentrated *in vacuo*. The residue was dissolved in MeCN (5 mL) and the pH value of the mixture was adjusted to 7~8 with NaHCO₃ before filtered. After that, BDP-Cl (100 mg) and Et₃N (200 μL) were added. After the reaction mixture was heated to 80 °C and stirred for 10 h, the solvent was removed *in vacuo* and residue was dissolved in DCM. The organic layer was washed with

saturated sodium chloride (3×10 mL), dried with sodium sulfate, and concentrated *in vacuo*. The residue was loaded onto a column of silica gel to give piperazine-substituent BODIPY (122 mg, 83% yield) as an orange solid.

(4-(4-(5,5-Difluoro-1,3,7,9-tetramethyl-5H-4λ⁴,5λ⁴-dipyrrolo[1,2-c:2',1'-f][1,3,2]diazaborinin-10-yl)benzyl)piperazin-1-yl)(3-hydroxypyridin-2-yl)methanone (**BDP-3**). Orange solid (183 mg, 36 % yield); ¹H NMR (400 MHz, CDCl₃) δ 11.81 (s, 1H), 8.11 (dd, *J* = 4.2, 1.6 Hz, 1H), 7.49 (d, *J* = 7.9 Hz, 2H), 7.38 – 7.25 (m, 4H), 4.46 (s, 2H), 3.88 (s, 2H), 3.66 (s, 2H), 2.58 (d, *J* = 9.1 Hz, 10H), 1.40 (s, 6H). ¹³C NMR (100 MHz, CDCl₃) δ 168.00, 158.47, 155.46, 142.99, 141.59, 138.57, 134.62, 134.05, 131.47, 129.78, 128.06, 127.43, 126.06, 121.24, 62.46, 53.67, 47.87, 43.15, 14.58, 14.36. ES-MS (ESI⁺, CH₃CN): Calcd for C₃₀H₃₂BF₂N₅O₂ [M+H]⁺ *m/z*=544.43, found *m/z*=544.39.

(4-(4-(5,5-Difluoro-1,3,7,9-tetramethyl-5H-4λ⁴,5λ⁴-dipyrrolo[1,2-c:2',1'-f][1,3,2]diazaborinin-10-yl)benzyl)piperazin-1-yl)(2-hydroxyphenyl)methanone (**BDP-4**). Orange solid (85 mg, 63% yield); ¹H NMR (400 MHz, CDCl₃) δ 9.63 (s, 1H), 7.48 (d, *J* = 6.7 Hz, 2H), 7.34 (d, *J* = 7.0 Hz, 1H), 7.27 (d, *J* = 6.7 Hz, 3H), 7.03 (d, *J* = 7.8 Hz, 1H), 6.88 (d, *J* = 6.7 Hz, 1H), 6.00 (s, 2H), 3.79 (s, 4H), 3.66 (s, 2H), 2.56 (d, *J* = 13.0 Hz, 10H), 1.39 (s, 6H). ¹³C NMR (100 MHz, CDCl₃) δ 170.82, 159.12, 155.49, 142.95, 141.52, 138.42, 134.12, 132.71, 131.45, 129.74, 128.33, 128.10, 121.25, 118.57, 118.14, 116.90, 62.42, 53.03, 29.70, 14.58, 14.35. ES-MS (ESI⁺, CH₃CN): Calcd for C₃₁H₃₃BF₂N₄O₂ [M+H]⁺ *m/z*=543.44, found *m/z*=543.35.

(4-(4-(5,5-Difluoro-1,3,7,9-tetramethyl-5H-4λ⁴,5λ⁴-dipyrrolo[1,2-c:2',1'-f][1,3,2]diazaborinin-10-yl)benzyl)piperazin-1-yl)(phenyl)methanone (**BDP-5**). Orange solid (122 mg, 83% yield); ¹H NMR (400 MHz, CDCl₃) δ 7.45 (d, *J* = 7.9 Hz, 2H), 7.41 (s, 5H), 7.23 (d, *J* = 7.9 Hz, 2H), 5.98 (s, 2H), 3.83 (s, 2H), 3.64 (s, 2H), 3.46 (s, 2H), 2.55 (s, 8H), 2.39 (s, 2H), 1.37 (s, 6H). ¹³C NMR (100 MHz, CDCl₃) δ 170.30, 155.42, 142.97, 141.60, 138.61, 135.85, 133.98, 131.46, 129.73, 128.49,

128.02, 127.04, 121.24, 62.47, 53.12, 47.78, 42.16, 14.57, 14.33. ES-MS (ESI⁺, CH₃CN): Calcd for C₃₁H₃₃BF₂N₄O [M+H]⁺ m/z=527.44, found m/z=527.45.

2.7 Preparation of BDP2-Br₂@mPEG nanoparticles

The nanoparticles were prepared using the same method as the literature reported [25]. DSPE-mPEG5000 (20 mg) was added, followed by the dissolution of BDP2-Br₂ (13 mg) in CHCl₃ (10 mL) at normal atmospheric temperature. The solution was stirred at room temperature for 10 min, and the solvent was removed in a vacuum. The residue was dissolved in PBS. Particles in the solution were then isolated by centrifugation at 8000 rpm for 20 min and dried at 40 °C to generate BDP2-Br₂@mPEG nanoparticles as red-purple solids. BODIPY content was up to 12.6 ± 1.0 wt % calculated on the basis of UV-vis absorption at 522 nm of BDP2-Br₂ in the supernatant (mean value based on three parallel results).

2.8 Determination of fluorescence quantum yield

The relative fluorescence quantum yields of the BODIPY derivatives were determined by comparison methods. The fluorescence quantum yield was calculated by the following equations:

$$\Phi = \Phi_S \times F/F_S \times A_S/A$$

Φ and Φ_S are the fluorescence quantum yields of the sample and the reference, F/F_S is the integral fluorescence intensity ratio of the sample and the reference, and A_S/A is the absorbance ratio of the reference and sample at the same excitation wavelength. The methoxyfluoroborazole (BDPOMe, $\Phi_S = 0.30/\text{MeCN}$) reported in the literature was used as the reference [26]. The excitation wavelength was 475 nm and the integrated area was from 480 nm to 700 nm when BODIPYs were tested.

2.9 Determination of transient fluorescence lifetime

The fluorescence lifetime of the compounds was determined using a time-dependent single photon counting setup (TCSPC) (Fluo Time 200, Picoquant GmbH) and a diode laser (LDH-P-670, PDL 800-B, Picoquant GmbH, 670 nm, 20 MHz, 44 ps), and fluorescence lifetime values and error analysis were calculated using FluorFit software.

2.10 Interaction with lipase

The affinity interaction of BODIPY derivatives to lipase were assayed using a fluorescence spectrofluorometer Model CARY Eclipse. The tryptophan present in pancreatic lipase (PL) was used as an intrinsic fluorophore ($\lambda_{ex} = 290$ nm; $\lambda_{em} = 340$ nm). The stock solution of PL was 0.5 mg/mL with distilled water. In several microtubes, the BODIPY derivatives (0 μ M to 60 μ M) in phosphate buffer (50 mM, pH 7.0), were mixed with PL (0.5 mg/mL) and allowed to react for 5 min. The emission spectrum of the mixture was measured. Since the BODIPY derivatives may possess intrinsic fluorescence at the λ_{ex} (290 nm), their spectra were measured and subtracted in all fluorescence experiments.

2.11 Singlet oxygen measurement

To assess whether the nanoparticle could generate singlet oxygen under LED light irradiation, following tests were carried out [25]. A 30 mL of constantly aerated acetonitrile solution containing BDP-2 (1 μ M) or BDP2-Br₂ (1 μ M), or BDP2-Br₂@mPEG (6 μ g/mL, its BDP2-Br₂ content: 1 μ M), or Rose Bengal (1 μ M) and 1, 3-diphenylisobenzofuran (DPBF) (50 μ M), was irradiated with a 4 W green LED light at 25°C for 10 min. Aliquots of 1 mL were taken from the solution every 1 min for 10 min, and then a UV-visible spectrum was recorded. 1,3-Diphenylisobenzofuran (DPBF) is a singlet oxygen quencher. The singlet oxygen produced by the nanoparticles under irradiation was confirmed by the decrease in UV absorbance of DPBF at 414 nm.

2.12 Cytotoxicity testing

The cytotoxicity assays were measured with BGC-823 cells in normal culture conditions. BGC-823 cells were seeded at a density of 5×10^3 cells per mL into sterile 96-well plates. Samples were dispersed in H₂O and diluted with culture media. The cytostatic effects of different concentration of BDP2-Br₂@mPEG nanoparticles (0 to 96 $\mu\text{g}/\text{mL}$) in the dark conditions or green LED light irradiation (4 W) for 120 min were measured. Cell viability was determined with the 3-[4,5-dimethylthiazol-2-yl]-2,5-diphenyltetrazoliumbromide (MTT) assay by measuring the absorbance at 570 nm. Each test was performed in triplicate.

2.13 Bacterial culture

All the equipments used in this experiment were sterilized before used. *E. coli* were chosen as the bacterial model to explore the antimicrobial activity of compounds and BDP2-Br₂@mPEG nanoparticles. A single colony of *E. coli* was used to inoculate 3 mL of Luria-Bertani (LB) medium and cells were grown at 37 °C under aerobic conditions on a shaker incubator (180 rpm) until an OD₆₀₀ nm of approximately 0.8 was reached. Cells were harvested by centrifugation (10 min, ~2000 g) and washed twice with PBS. The cells were then resuspended in PBS and diluted to $\sim 10^6$ CFU·mL⁻¹ for antibacterial assays and photodynamic inactivation assay.

2.14 Antibacterial assays

Gram-negative Escherichia coli (*E. coli*) strain was purchased from Shanghai Luwei Technology Co., Ltd. The bacteria were cultured in LB broth medium. The bacterial concentration was monitored by measuring the OD value of the bacteria at 600 nm. All assays were conducted in 96-well, flat bottom, sterile plates. Bacterial suspension was adjusted to contain 1×10^6 CFU/mL in fresh sterile PBS solution. Five compounds (1 μM to 16 μM) and BDP2-Br₂@mPEG (6 $\mu\text{g}/\text{mL}$ to 96 $\mu\text{g}/\text{mL}$, its BDP2-Br₂ content: 1 μM to 16 μM) were transferred into the assay plate, respectively. Next, the plates were serially twofold diluted in triplicate, and 100 μL of the bacterial solution was added (final

inculum 5×10^5 CFU/mL). The final volume for the assay was 200 μ L. The control groups were set without compounds for each assay. Each test was performed in triplicate. Plates were incubated in a plate shaker (200 rpm) at 37 °C for 24 h. The above operation is carried out in a clean bench. Then the absorbance at 600 nm of bacterial suspension was measured. The inhibition rate on *E. coli* was calculated by the following formula:

$$\text{Inhibition Rate (\%)} = (C_{\text{OD600}} - T_{\text{OD600}}) C_{\text{OD600}} / \times 100 \%$$

where C_{OD600} and T_{OD600} represent the absorbance at 600 nm in the control group and the treatment group, respectively.

2.15 Photodynamic inactivation assay

Photodynamic inactivation assay was carried out as previously reported [26]. The BDP2-Br₂@mPEG solutions (96, 48, 24, 12, 6 and 0 μ g/mL) were mixed with the same volume of bacterial suspension (1×10^6 CFU/mL). After 10 min of static incubation at 37 °C in the dark, the cultures were irradiated with the green LED device (4 W) for 1 h. Survivors were quantified using the viable count technique. Plates were then incubated for 24 h at 37 °C. For each experiment the following controls were set: samples exposed to the photosensitizer and not irradiated (+PS, -light), samples without the photosensitizer and irradiated (-PS, +light), samples without the photosensitizer and not irradiated (-PS, -light), samples exposed to DSPE-mPEG and irradiated (+DSPE-mPEG, +light) and samples exposed to DSPE-mPEG and not irradiated (+DSPE-mPEG, -light). For each test three independent experiments were carried out.

2.16 Release of cytoplasmic constituents

The cytoplasmic constituents such as DNA and RNA have strong absorption at 260 nm, therefore the release of the cytoplasmic constituents from the bacteria can be monitored by their strong absorption at 260 nm [27]. The concentration of *E. coli* was adjusted to $\text{OD}_{600}=1.0$, centrifugated and washed with PBS three times. Then, the bacteria were incubated with the

BDP2-Br₂@mPEG under green LED light (5 W) for 60 min, the samples in the dark conditions were used as control. Finally, the bacterial suspensions were filtered with 220 nm syringe filters immediately to remove the bacteria, and optical density at 260 nm was recorded. Each test was performed in triplicate.

2.17 Preparation of bacterial samples for SEM

E. coli suspension and *E. coli* suspension treated with BDP2-Br₂@mPEG under irradiation (1 mL, 1×10^6 CFU/mL) were collected. All bacterial suspensions were placed on the slide, fixed with glutaraldehyde for 12 h, dried in a freeze-dryer (Flexi-Dry™ MP), gold sputter-coated, and imaged using a scanning electron microscope (SEM, Shimadzu SS-550).

3. Results and discussion

3.1 Syntheses and characterizations

Five functional groups BODIPY conjugates were synthesized by electrophilic substitution or amide condensation respectively (Scheme 1a and Scheme S1). BDP2-Br₂ was synthesized by bromination with NBS. The ¹H NMR, ¹³C NMR and MS spectra of the compounds confirm the compounds with exact structures and high purity (Fig. S1-S18). To enhance solubility of BDP2-Br₂ in water, DSPE-mPEG5000 was used to produce nanoself-assembly of BDP2-Br₂@mPEG by hydrophilic and hydrophobic interactions (Scheme 1b). BDP2-Br₂@mPEG has a cuboid structure (Figure 1a), which can be dispersed uniformly with an average diameter of 262.1 nm (Fig. 1b), confirming that the BDP2-Br₂ self-assembled into nanoscaled cuboids with DSPE-mPEG in aqueous solutions. The UV-vis absorption of BDP2-Br₂@mPEG is in the range of 500-600 nm, which red shifted compared to BDP2-Br₂. This indicates that the nanoparticles can absorb visible light (Fig. 1c, Fig. S19). The maximum emission wavelength of BDP2-Br₂@mPEG shifted to the infrared region compared to BDP-2 and BDP2-Br₂ (Fig. 1d, Fig. S20).

Scheme 1. (a) Chemical structures of the five BODIPYs and BDP2-Br₂ and (b) Schematic illustration of the synthesis and antibacterial mechanism of BDP2-Br₂@mPEG nanoparticles.

Fig. 1. Characterization of BDP2-Br₂ and BDP2-Br₂@mPEG nanoparticles. (a) SEM image of BDP2-Br₂@mPEG. (b) Diameter sizes of the BDP2-Br₂@mPEG nanoparticles as measured by dynamic light scattering. (c) UV-vis spectra of BDP2-Br₂ (10 μM, MeCN) and BDP2-Br₂@mPEG (50 μg/mL, H₂O). (d) Excitation and emission spectra of BDP2-Br₂@mPEG (25 μg/mL, H₂O).

3.2 Spectroscopic properties of BODIPYs

The fluorescence emission and fluorescence quantum yield of BDP derivatives were measured (Table 1). The emission wavelength of the BDP2-Br₂ is 535 nm and its stock shift ($\Delta\lambda = \lambda_{em} - \lambda_{ex}$) is 9 nm (Table 1). What's more, the maximum emission of BDP2-Br₂@mPEG is 545 nm, and its stock shift (18 nm), which is two times higher than BDP2-Br₂, indicating the existence of π - π interaction and intramolecular charge transfer in BDP2-Br₂@mPEG [30]. The methoxy-substituted BODIPY (BDPOMe, $\Phi_S = 0.30/\text{MeCN}$) reported in the literature was used as a reference for the determination of fluorescence quantum yield [26]. The results show that the fluorescence quantum yields of the five non-brominated derivatives except BDP-1 are similar to that of BDPOMe, with values ranging from 0.30 to 0.31, indicating less effect of substitutes on the emission of BODIPY core. The fluorescence quantum yield of BDP-1 is lower than that of other BODIPY derivatives because of the nitro group quenching effect. Also, the fluorescence quantum yield of BDP2-Br₂ was reduced because of the heavy atom effect. The fluorescence lifetime of compounds was determined using a time-dependent single photon technique to investigate the transient changes in fluorescence (Fig. S21). The attenuation curve integral was obtained by FluorFit software simulation under normal temperature

test conditions. As shown in Table 1, the fluorescence lifetimes of the compounds BDP-2, BDP-3, BDP-4 and BDP-5 are longer than that of BDP-1. The life time (3.93 ns) of BDP-3 is longer than others, indicating that the chain in the body of BODIPY has effects on its life time.

Table 1. Spectroscopic properties of BODIPYs at room temperature

3.3 Affinity to lipase

Porcine pancreatic lipase (PL) consists of more than 400 amino acid residues in a single polypeptide of globular shape which contains seven tryptophans with intrinsic fluorescence. The addition of BODIPY derivatives to lipase caused a reduction of protein fluorescence intensity ($\lambda_{em}=362$ nm) known as quenching effect (Fig. 2a). It was assumed that the interaction between the enzyme and BODIPY derivatives did not significantly change the environment of the tryptophan residues since the shape of the protein spectra did not change [31]. The decrease in fluorescence intensity indicates the strong interaction between the compounds and the lipase. As shown in Fig. 2b, BDP-2 is the one that decreased the fluorescence intensity of tryptophan residues in lipase significantly, which means that BDP-2 has a good affinity to lipase. It was reported that lipase was widely found in the out membrane of *E. coli* [32], which was used as a standard model for lipase-targeting compounds to achieve an easier way of bacteriostasis with good effects [33]. Based on this feature, we chose BDP-2 as the delicate compound for bromination in order to enhance its ability of generating 1O_2 . DSPE-mPEG was then used to produce water dispersible nanoparticles with BDP-2 by hydrophobic interactions.

Fig. 2. Emission spectra of PL (0.5 mg/mL, H₂O) in the presence of various amount of BODIPYs; (a) BDP-2 (a to g: 0, 10, 20, 30, 40, 50, 60 μ M); The exciting wavelength was 290 nm. (b) Fluoresce

intensity changes of PL at 334 nm in the presence of BODIPYs (60 μM) (A, BDP-1; B. BDP-2; C. BDP-3; D. BDP-4; E. BDP-5)

3.4 Generation of singlet oxygen

The rate of singlet oxygen generation is an important parameter for an aPDI reagent. Rose Bengal was used as a positive control, which is considered to be one of the powerful singlet oxygen generators under irradiation [34]. Singlet oxygen was measured by monitoring the absorption decrease of DPBF at 414 nm. As was shown in Fig. 3, the BDP-2 had little effect on DPBF under green LED light irradiation, while the BDP2-Br₂ and BDP2-Br₂@mPEG caused obvious absorption decrease of DPBF at 414 nm. This means the generation of ¹O₂ because of the heavy atom effect. The relative rate of DPBF degradation under given conditions is in a ratio of 1:0.80:0.66:0.04 for Rose Bengal:BDP2-Br₂:BDP2-Br₂@mPEG:BDP-2, where Rose Bengal is generally considered to be a powerful substance that produces ¹O₂ fast. The results indicate that the BDP2-Br₂@mPEG can generate ROS and has the potential to be an excellent aPDI agent.

Fig. 3. (a) DPBF degradation profiles in 8 min by BDP2-Br₂@mPEG (Insert: Changes of absorbance at 414 nm); (b) Comparative reactive oxygen species generation rates plot for BDP-2 (A), BDP2-Br₂@mPEG (B), BDP2-Br₂ (C) and Rose Bengal (D). The concentration of all photosensitizers was at 1×10^{-6} M, and DPBF was initially at 5×10^{-5} M in acetonitrile. The slopes (m) and the R² coefficients of the lines are determined by linear regression.

3.5 Cytotoxicity testing

The inhibitory effect of BDP2-Br₂@mPEG on the growth of BGC-823 cells was determined by MTT reduction method. Experimental results demonstrate that BDP2-Br₂@mPEG does not show

significant cytostatic effects without irradiation (Fig. 4). Conversely, BDP2-Br₂@mPEG exhibits an obvious cytotoxicity under illumination and its IC₅₀ is 18.3 µg/mL. This indicates that the cytotoxicity of BDP2-Br₂@mPEG is initiated by green LED light irradiation. The results indicate that the BDP2-Br₂@mPEG is low-toxicity without irradiation.

Fig 4. Cytotoxicity of different concentrations of BDP2-Br₂@mPEG to BGC-823 cells in dark conditions and green LED light for 120 min. The results are represented as mean ± SD (n = 3). The *t*-test revealed the statistical significance of samples in the dark and samples illuminated with green LED light with respect to control sample. Statistical significance is denoted by * ($p < 0.05$), ** ($p < 0.005$), *** ($p < 0.001$), and **** ($p < 0.0001$).

3.6 Antibacterial assays

To compare the antimicrobial properties of five compounds, the following antibacterial assays were conducted. As shown in Fig. 5, the inhibition rates of all non-brominated compounds on *E. coli* is below 5% at low concentrations (1 µM to 4 µM), and as the concentration of compounds increases, BDP-2, BDP-3 and BDP2-Br₂@mPEG show the relatively higher inhibition rate on *E. coli*, in which the BDP-2 shows the highest inhibition rate of 48.2 ± 7.9 %. The antibacterial activity of BDP2-Br₂@mPEG nanoparticles was slightly reduced, which may be caused by DSPE-mPEG encapsulation. Therefore, we believe that BDP2-Br₂@mPEG will have a good antibacterial effect among these compounds and can be a promising choice for antimicrobial dyes because BDP2-Br₂@mPEG nanoparticles has better water solubility and can also generate ¹O₂.

Fig. 5. Inhibition rates of five compounds (1 μM to 16 μM) and BDP2-Br₂@mPEG (6 $\mu\text{g/mL}$ to 96 $\mu\text{g/mL}$, its BDP2-Br₂ content: 1 μM to 16 μM) on *E. coli*. Data are expressed as the mean from three independent experiments performed in triplicate.

The photo-induced antibacterial activity of the nanoparticles was evaluated. The light dose was fixed (green LED, 500 nm). Various concentration of the BDP2-Br₂@mPEG nanoparticles (0, 6, 12, 24, 48, 96 $\mu\text{g/mL}$) were investigated and controls including samples exposed to the photosensitizer and not irradiated (+PS, -light), samples without the photosensitizer and irradiated (-PS, +light), samples without the photosensitizer and not irradiated (-PS, -light), samples exposed to DSPE-mPEG and irradiated (+DSPE-mPEG, +light) and samples exposed to DSPE-mPEG and not irradiated (+DSPE-mPEG, -light), were set (Figure S22). Results show that untreated *E. coli* could grow normally and its growth was slightly influenced by the green LED light irradiation. The number of bacteria decreased a lot when the BDP2-Br₂@mPEG nanoparticles were added. The adamantane derivatives were reported to be active against drug-susceptible and drug-resistant TB strains [35]. Experimental results indicate that the toxicity of the nanoparticles was not caused by DSPE-mPEG (Fig. S22e and S22f). We propose that the antibacterial property of BDP2-Br₂@mPEG was due to the dark-cytotoxicity from the adamantane group. Furthermore, the concentration effect of BDP2-Br₂@mPEG on the photodynamic inactivation of *E. coli* was investigated (Fig. 6). As expected, the inhibition of BDP2-Br₂@mPEG to *E. coli* is dose-dependent. The number of survivors was reduced by 5 log units when the concentration of BDP2-Br₂@mPEG was increased from 0 to 24 $\mu\text{g/mL}$. When the concentration of the nanoparticles continued to double, there were no visible colonies.

Fig. 6. Effects of increasing concentrations of BDP2-Br₂@mPEG on the photodynamic inactivation of *E. coli*. Light dose: 5 J/cm². Data are expressed as the means of three independent experiments ± SD.

Previous studies reported that the bacterial apoptosis is associated with bacterial membrane damage [36, 37]. In this work, absorption study at 260 nm was used to confirm whether the membrane of *E. coli* was broken. Absorption at 260 nm of the bacteria incubated with BDP2-Br₂@mPEG under illumination is higher than the bacteria under dark condition (Fig. 7). The result indicates that the membrane of more bacteria was broken and the cytoplasmic constituents inside had leaked out under irradiation.

Fig. 7. Absorption at 260 nm of *E. coli* after incubated with BDP2-Br₂@mPEG under dark and LED light. The results are represented as mean ± SD (n = 3).

SEM images were used to illustrate the antibacterial effect of the BDP2-Br₂@mPEG nanoparticles. The morphology of the bacteria treated with nanoparticles shows significant changes after illumination compared to the control group (without nanoparticles) (Fig. 23). Distorted bacterial walls can be clearly observed after illumination compared to the smooth surface of control cells. The membrane of bacterial cell was severely damaged by ¹O₂ so that most of them were broken. This led to an irreversible destruction of the membrane structure of the bacteria, indicating that the bacteria were dead.

4. Conclusions

In this work, five functional groups (such as benzamide, adamantane, etc.) conjugated BODIPY were synthesized and characterized. Lipase affinity and antibacterial assays were conducted by spectroscopic methods. The spectroscopic features of BODIPY derivatives for lipases affinity and

antibacterial activity were reported. Lipase affinity assay results indicate that BDP-2 was the most active compound among the five compounds. Therefore, BDP-2 was used to synthesize photoresponsive nanoparticle (BDP2-Br₂@mPEG). BDP2-Br₂@mPEG was very active against *E. coli* under illumination, making it a very promising aPDI agent. Our results confirm that functional group conjugated BODIPY would be potential visible light driven antibacterial dyes. Visible light is healthy to human. Bacterial targeting photodriven antibacterial materials will be new green materials for the sustainable treatment of bacteria.

Conflicts of interest

There are no conflicts to declare.

Acknowledgements

This work was financially supported by the National Science Foundation of China (21571085).

References

- [1] P. Picconi, C. Hind, S. Jamshidi, K. Nahar, M. Clifffford, M.E. Wand, J.M. Sutton, K.M. Rahman, Triaryl benzimidazoles as a new class of antibacterial agents against resistant pathogenic microorganisms, *J. Med. Chem.* 60 (2017) 6045-6059.
- [2] Z.W. Chen, Z.Z. Wang, J.S. Ren, Enzyme mimicry for combating bacteria and biofilms, *Acc. Chem. Res.* 51 (2018)789-799.
- [3] L. Garcia-Migura, R.S. Hendriksen, L. Fraile, F.M. Aarestrup, Antimicrobial resistance of zoonotic and commensal bacteria in Europe: the missing link between consumption and resistance in veterinary medicine, *Vet. Microbiol.* 170 (2014) 1-9.

- [4] Y. Hu, T.Y. Zhang, L. Jiang, S.J. Yao, H. Ye, K.F. Lin, C.Z. Cui, Removal of sulfonamide antibiotic resistant bacterial and intracellular antibiotic resistance genes by UVC-activated peroxymonosulfate, *Chem. Eng. J.* 368 (2019) 888-895.
- [5] C.Y. Mao, Y.M. Xiang, X.M. Liu, Y.F. Zheng, K.W.K. Yeung, Z.D. Cui, X.J. Yang, Z.Y. Li, Y.Q. Liang, S.L. Zhu, S.L. Wu, Local photothermal/photodynamic synergistic therapy by disrupting bacterial membrane to accelerate reactive oxygen species permeation and protein leakage, *ACS Appl. Mater. Interfaces* 11 (2019) 17902-17914.
- [6] J. Shi, Z. Chen, L. Wang, B. Wang, L. Xu, L. Hou, Z. Zhang, A tumor-specific cleavable nanosystem of PEG-modified C60@Au hybrid aggregates for radio frequency-controlled release, hyperthermia, photodynamic therapy and X-ray imaging, *Acta Biomater.* 29 (2016) 282-297.
- [7] X.L. Fang, R. Akrofi, H. Yang, Q.Y. Chen, The NIR inspired nano-CuSMn(II) composites for lactate and glycolysis attenuation, *Colloids Surf., B* 181 (2019) 728-733.
- [8] M.L. Agazzi, M.B. Ballatore, E. Reynoso, E.D. Quiroga, E.N. Durantini, Synthesis, spectroscopic properties and photodynamic activity of two cationic BODIPY derivatives with application in the photoinactivation of microorganisms, *Eur. J. Med. Chem.* 126 (2017) 110-121.
- [9] F. Vatansever, W.C.de Melo, P. Avci, D. Vecchio, M. Sadasivam, A. Gupta, R. Chandran, M. Karimi, N.A. Parizotto, R. Yin, G.P. Tegos, M.R. Hamblin, Antimicrobial strategies centered around reactive oxygen species - bactericidal antibiotics, photodynamic therapy, and beyond, *FEMS Microbiol. Rev.* 37 (2013) 955-989.
- [10] A. Turksoy, D. Yildiz, E.U. Akkaya, Photosensitization and controlled photosensitization with BODIPY dyes. *Coord. Chem. Rev.* 279 (2019) 47-64.

- [11] X. Dai, X. Chen, Y. Zhao, Y. Yu, X. Wei, X. Zhang, C. Li, A Water-Soluble galactose-decorated cationic photodynamic therapy agent based on BODIPY to selectively eliminate biofilm, *Biomacromol.* 19 (2018) 141-149.
- [12] Y.J. Xu, M.L. Zhao, L. Zou, L.C. Wu, M.J. Xie, T.S. Yang, S.J. Liu, Q. Zhao, Local photothermal/photodynamic synergistic therapy by disrupting bacterial membrane to accelerate reactive oxygen species permeation and protein leakage, *ACS Appl. Mater. Interfaces* 10 (2018)44324-44335.
- [13] W.L. Lu, Y.Q. Lan, K.J. Xiao, Q.M. Xu, L.L. Qu, Q.Y. Chen, T. Huang, J. Gao, Y.J. Zhao, BODIPY-Mn nanoassemblies for accurate MRI and phototherapy of hypoxia cancer, *Mater. Chem. B* 5 (2017) 1275-1283.
- [14] A. Alabugin, Near-IR Photochemistry for Biology: Exploiting the Optical Window of Tissue, *Photochem. Photobiol.* 95 (2019) 722-732.
- [15] E.Caruso, S. Banfifi, P. Barbieri, B. Leva, V.T. Orlandi, Synthesis and antibacterial activity of novel cationic BODIPY photosensitizers, *Photochem. Photobiol. B* 114 (2012) 44-51.
- [16] I.O. Bacellar, C. Pavani, E.M. Sales, R. Itri, M. Wainwright, M.S. Baptista, Membrane damage efficiency of phenothiazinium photosensitizers, *Photochem. Photobiol.* 90 (2014) 801-813.
- [17] M.V. Buchieri, M. Cimino, S. Rebollo-Ramirez, C. Beauvineau, A. Cascioferro, S. Favre-Rochex, O. Helynck, D. Naud-Martin, G. Larrouy-Maumus, H. Munier-Lehmann, B. Gicquel, Nitazoxanide analogs require nitroreduction for antimicrobial activity in mycobacterium smegmatis, *J. Med. Chem.* 60 (2017) 7425-7433.
- [18] P.L. Zhang, Z.K. Wang, Q.Y. Chen, X. Du, J. Gao, Biocompatible G-Quadruplex/BODIPY assembly for cancer cell imaging and the attenuation of mitochondria, *Bioorg. Med. Chem. Lett.* 29 (2019) 1943-1947.

- [19] J. Odingo, M.A. Bailey, M. Files, J.V. Early, T. Alling, D. Dennison, J. Bowman, In vitro evaluation of novel nitazoxanide derivatives against mycobacterium tuberculosis, *ACS Omega* 9 (2017) 5873-5890.
- [20] M. A. Tabrizi, P. G. Baraldi, S. Baraldi, E. Ruggiero, L. D. Stefano, F. Rizzolio, L. D. C. Mannelli, C. Ghelardini, A. Chicca, M. Lapillo, J. Gertsch, C. Manera, M. Macchia, A. Martinelli, C. Granchi, F. Minutolo, T. Tuccinardi, Discovery of 1,5-diphenylpyrazole-3-carboxamide derivatives as potent, reversible, and selective monoacylglycerol lipase (MAGL) inhibitors, *J. Med. Chem.* 2018, 61: 1340-1354.
- [21] H. Deng, S. Kooijman, A. M. C. H. v. d. Nieuwendijk, D. Ogasawara, T. Wel, F. v. Dalen, M. P. Baggelaar, F. J. Janssen, R. J. B. H. N. v. d. Berg, H. d. Dulk, B. F. Cravatt, H. S. Overkleeft, P. C. N. Rensen, M. v. d. Stelt, Triazole ureas act as diacylglycerol lipase inhibitors and prevent fasting-induced refeeding, *J. Med. Chem.* 2017, 60, 428-440
- [22] P.L. Zhang, J. Shao, X.T. Li, L.L. Qu, A protein amantadine-BODIPY assembly as the turn-on sensor of free copper (II), *Anal. Methods* 11(2019) 827-831.
- [23] Y.Q. Lan, K.J. Xiao, Y.J. Wu, Q.Y. Chen, Characterization, catalyzed water oxidation and anticancer activities of a NIR BODIPY-Mn polymer, *Spectrochim. Acta, Part A*, 177 (2017) 28-32.
- [24] C. Shao, X. Wang, J. Xu, J. Zhao, Q. Zhang, Y. Hu, Carboxylic acid-promoted copper(I)-catalyzed azide-alkyne cyclo addition, *J. Org. Chem.* 75 (2010) 7002-7005.
- [25] X. Du, P.L. Zhang, H.X. Fu, H.M. Ahsan, J. Gao, Q.Y. Chen, Smart mitochondrial-targeted cancer therapy: Subcellular distribution, selective TrxR2 inhibition accompany with declined antioxidant capacity, *Int. J. Pharm.* 555 (2019) 346-355.

- [26] W.B. Hu, Y.H. Lin, X.F. Zhang, M. Feng, S.W. Zhao, J. Zhang, Heavy-atom-free charge transfer photosensitizers: tuning the efficiency of BODIPY in singlet oxygen generation via intramolecular electron donor-acceptor interaction, *Dyes Pigm.* 164 (2019) 139-147.
- [27] D.O. Frimannsson, M. Grossi, J. Murtagh, F. Paradisi, D.F. O'Shea, Light induced antimicrobial properties of a brominated boron difluoride (BF₂) chelated tetraarylazadipyrromethene photosensitizer, *J. Med. Chem.* 53 (2010) 7337-7343.
- [28] J.Y. Lu, P.L. Zhang, Q.Y. Chen. A nano-BODIPY encapsulated zeolitic imidazolate framework as photoresponsive integrating antibacterial agent, *ACS Appl. Bio Mater.* 3 (2020) 458-465.
- [29] S. Liu, L. Wei, L. Hao, N. Fang, M.W. Chang, R. Xu, Y. Yang, Y. Chen, Sharper and faster “nano darts” kill more bacteria: a study of antibacterial activity of individually dispersed pristine single-walled carbon nanotube, *ACS Nano* 12 (2009) 3891-3902.
- [30] W.Y. Xiao, P. Wang, C.J. Ou, X.Y. Huang, Y.Y. Tang, M.Y. Wu, W.L. Si, J.J. Shao, W. Huang, X.C. Dong, 2-Pyridone-functionalized aza-BODIPY photosensitizer for imaging-guided sustainable phototherapy, *Biomater.* 183 (2018) 1-9.
- [31] A. Papadopoulou, R.J. Green, R.A. Frazier, Interaction of flavonoids with bovine serum albumin: A fluorescence quenching study, *J. Agric. Food Chem.* 53 (2005) 158-163.
- [32] K.E. Jaeger, T. Eggert, Lipases for biotechnology, *Curr. Opin. Biotechnol.* 13 (2002) 390-397.
- [33] H. Chen, Y. Jin, J. Wang, Y. Wang, W. Jiang, H. Dai, S. Pang, L. Lei, J. Ji, B. Wang, Design of smart targeted and responsive drug delivery systems with enhanced antibacterial properties, *Nanoscale* 10 (2018) 20946-20962.
- [34] I.E. Kochevar, R.W. Redmond, Photosensitized production of singlet oxygen, *Methods Enzymol.* 319 (2000) 20-28.

- [35] L. Jia, J.E. Tomaszewski, C. Hanrahan, L. Coward, P. Noker, G. Gorman, B. Nikonenko, M. Protopopova, Pharmacodynamics and pharmacokinetics of SQ109, a new diamine-based antitubercular drug, *Br. J. Pharmacol.* 144 (2005) 80-87.
- [36] W.Y. Mu, A. Robertson, Q.Y. Chen, Near-infrared-driven Au-decorated polymer-metal protein microfibers with bacterial filtration ability for use in photothermal sterilization, *Chem. Eng. J.* 388 (2020) 124236-124245.
- [37] Z.T. Lu, X.G. Zhang, Y. Zhao, Y.N. Xue, T.T. Zhai, Z.M. Wu, C.X. Li, BODIPY-based macromolecular photosensitizer with cation enhanced antibacterial activity, *Polym. Chem.* 6 (2015) 302-310.

Scheme 1. (a) Chemical structures of the five BODIPYs and BDP2-Br₂ and (b) Schematic illustration of the synthesis and antibacterial mechanism of BDP2-Br₂@mPEG nanoparticles.

Fig. 1. Characterization of BDP2-Br₂ and BDP2-Br₂@mPEG nanoparticles. (a) SEM image of BDP2-Br₂@mPEG. (b) Diameter sizes of the BDP2-Br₂@mPEG nanoparticles as measured by dynamic light scattering. (c) UV-vis spectra of BDP2-Br₂ (10 μM, MeCN) and BDP2-Br₂@mPEG (50 μg/mL, H₂O). (d) Excitation and emission spectra of BDP2-Br₂@mPEG (25 μg/mL, H₂O).

Fig. 2. Emission spectra of PL (0.5 mg/mL, H₂O) in the presence of various amount of BODIPYs; (a) BDP-2 (a to g: 0, 10, 20, 30, 40, 50, 60 μM); The exciting wavelength was 290 nm. (b) Fluorescence intensity changes of PL at 334 nm in the presence of BODIPYs (60 μM) (A, BDP-1; B, BDP-2; C, BDP-3; D, BDP-4; E, BDP-5).

Fig. 3. (a) DPBF degradation profiles in 8 min by BDP2-Br₂@mPEG (Insert: Changes of absorbance at 414 nm); (b) Comparative reactive oxygen species generation rates plot for BDP-2 (A), BDP2-Br₂@mPEG (B), BDP2-Br₂ (C) and Rose Bengal (D). The concentration of all

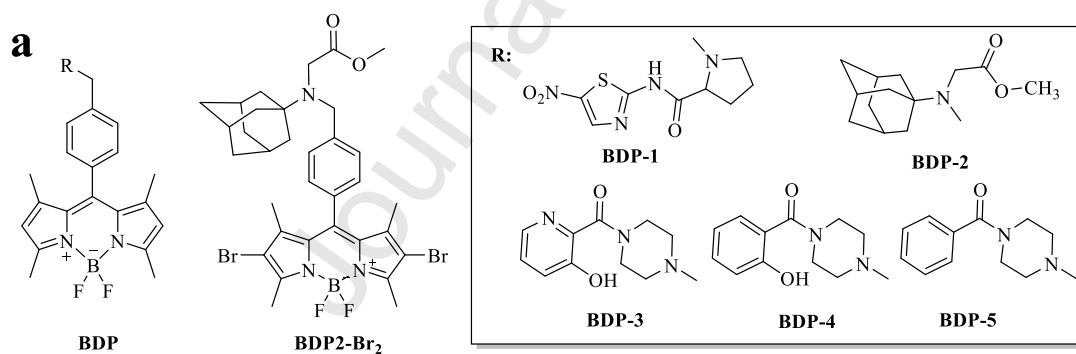
photosensitizers was at 1×10^{-6} M, and DPBF was initially at 5×10^{-5} M in acetonitrile. The slopes (m) and the R^2 coefficients of the lines are determined by linear regression.

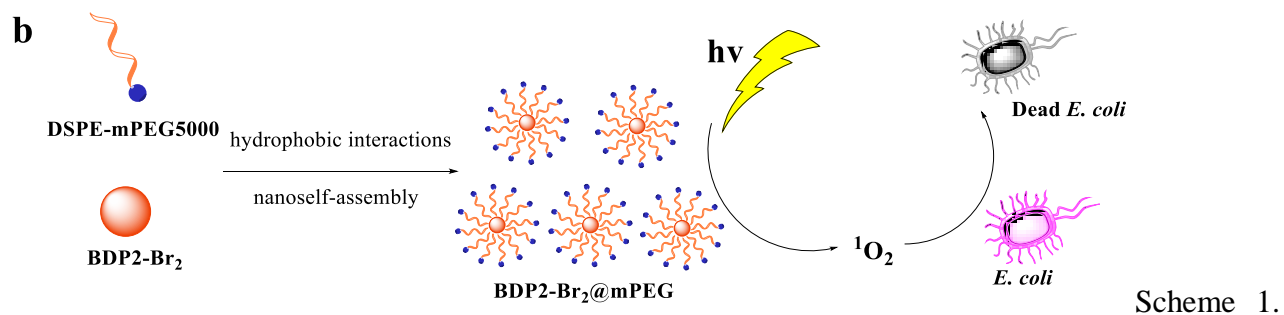
Fig 4. Cytotoxicity of different concentrations of BDP2-Br₂@mPEG to BGC-823 cells in dark conditions and green LED light for 120 min. The results are represented as mean \pm SD (n = 3). The *t*-test revealed the statistical significance of samples in the dark and samples illuminated with green LED light with respect to control sample. Statistical significance is denoted by * ($p < 0.05$), ** ($p < 0.005$), *** ($p < 0.001$), and **** ($p < 0.0001$).

Fig. 5. Inhibition rates of five compounds (1 μ M to 16 μ M) and BDP2-Br₂@mPEG (6 μ g/mL to 96 μ g/mL, its BDP2-Br₂ content: 1 μ M to 16 μ M) on *E. coli*. Data are expressed as the mean from three independent experiments.

Fig. 6. Effects of increasing concentrations of BDP2-Br₂@mPEG on the photodynamic inactivation of *E. coli*. Light dose: 5 J/cm². Data are expressed as the means of three independent experiments \pm SD.

Fig. 7. Absorption at 260 nm of *E. coli* after incubated with BDP2-Br₂@mPEG under dark and LED light. The results are represented as mean \pm SD (n = 3).





(a) Chemical structures of the five BODIPYs and BDP2-Br₂ and (b) Schematic illustration of the synthesis and antibacterial mechanism of BDP2-Br₂@mPEG nanoparticles.

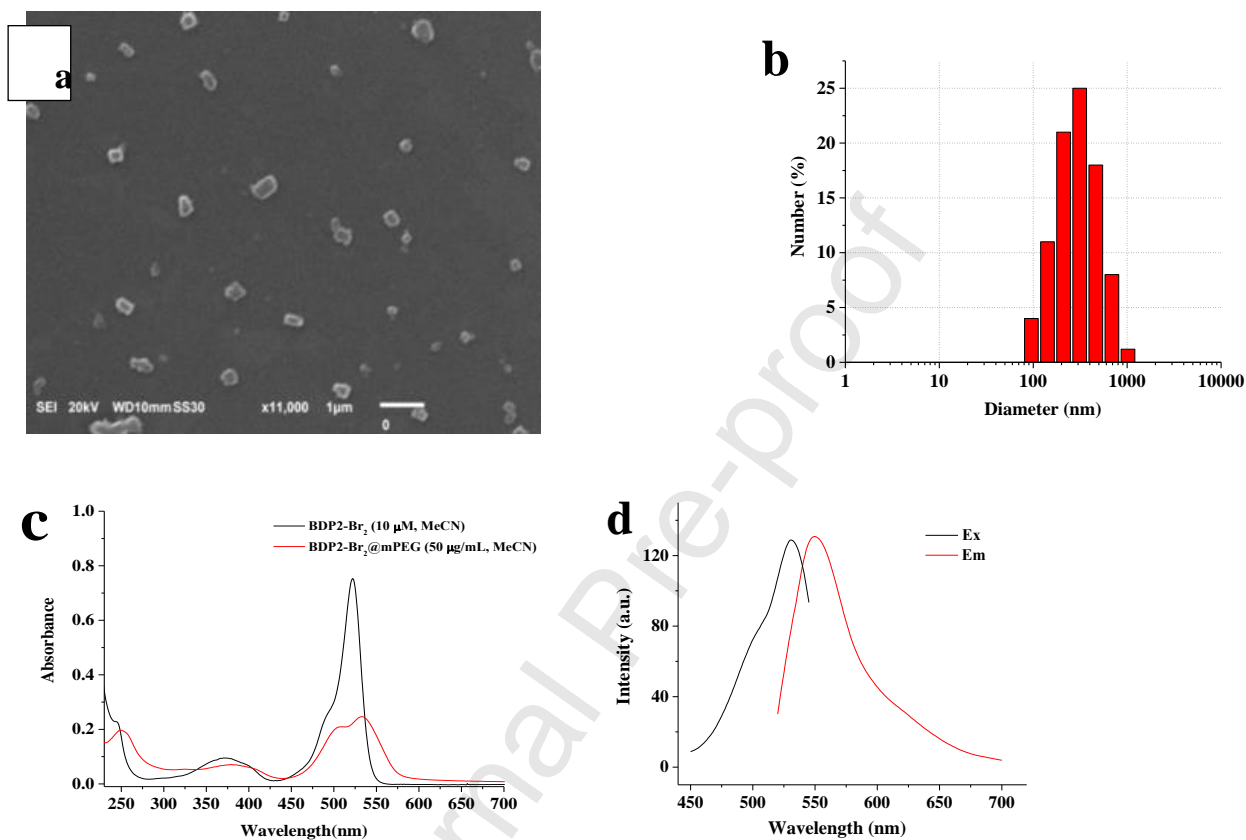


Fig. 1. Characterization of BDP2-Br₂ and BDP2-Br₂@mPEG nanoparticles. (a) SEM image of BDP2-Br₂@mPEG. (b) Diameter sizes of the BDP2-Br₂@mPEG nanoparticles as measured by dynamic light scattering. (c) UV-vis spectra of BDP2-Br₂ (10 μM, MeCN) and BDP2-Br₂@mPEG (50 μg/mL, H₂O). (d) Excitation and emission spectra of BDP2-Br₂@mPEG (25 μg/mL, H₂O).

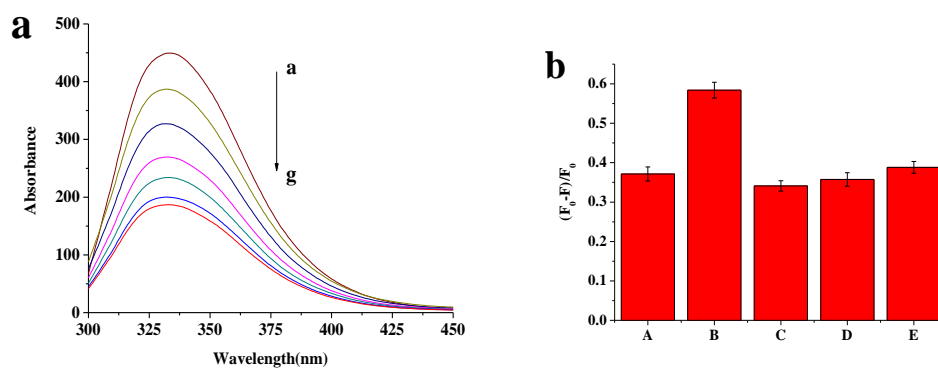


Fig. 2. Emission spectra of PL (0.5 mg/mL, H₂O) in the presence of various amount of BODIPYs; (a) BDP-2 (a to g: 0, 10, 20, 30, 40, 50, 60 μM); The exciting wavelength was 290 nm. (b) Fluorescence intensity changes of PL at 334 nm in the presence of BODIPYs (60 μM) (A, BDP-1; B. BDP-2; C. BDP-3; D. BDP-4; E. BDP-5).

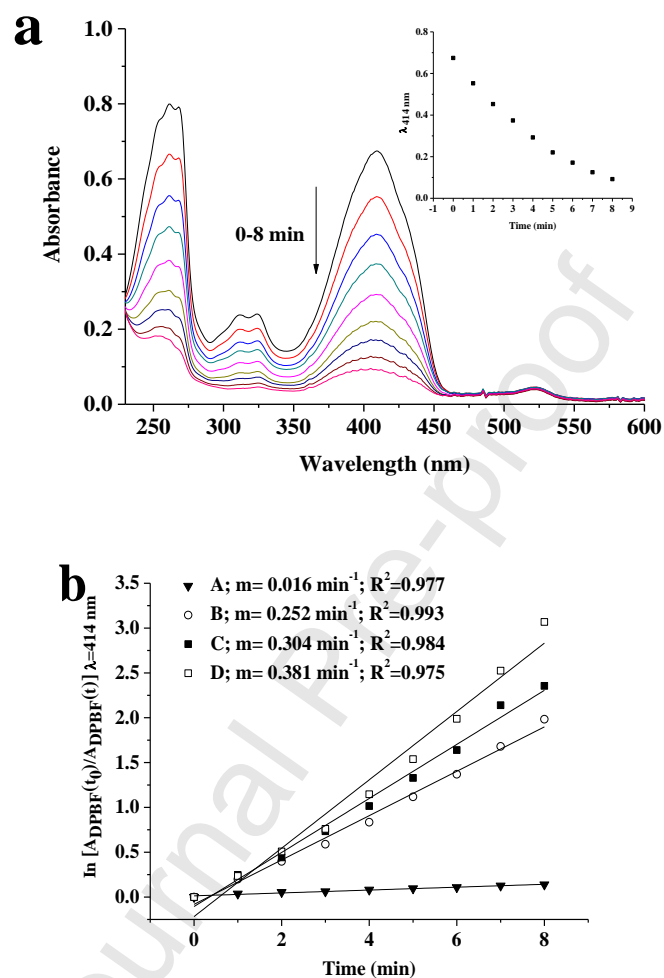


Fig. 3. (a) DPBF degradation profiles in 8 min by BDP2-Br₂@mPEG (Insert: Changes of absorbance at 414 nm); (b) Comparative reactive oxygen species generation rates plot for BDP-2 (A), BDP2-Br₂@mPEG (B), BDP2-Br₂ (C) and Rose Bengal (D). The concentration of all photosensitizers was at 1×10^{-6} M, and DPBF was initially at 5×10^{-5} M in acetonitrile. The slopes (m) and the R^2 coefficients of the lines are determined by linear regression.

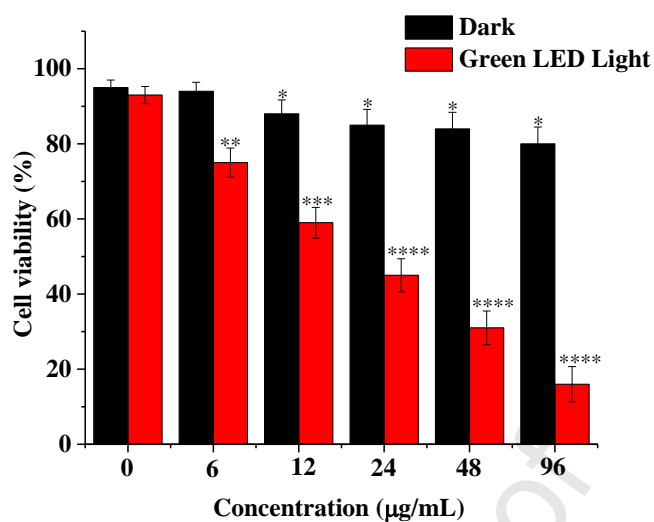


Fig 4. Cytotoxicity of different concentrations of BDP2-Br₂@mPEG to BGC-823 cells in dark conditions and green LED light for 120 min. The results are represented as mean \pm SD (n = 3). The *t*-test revealed the statistical significance of samples in the dark and samples illuminated with green LED light with respect to control sample. Statistical significance is denoted by * ($p < 0.05$), ** ($p < 0.005$), *** ($p < 0.001$), and **** ($p < 0.0001$).

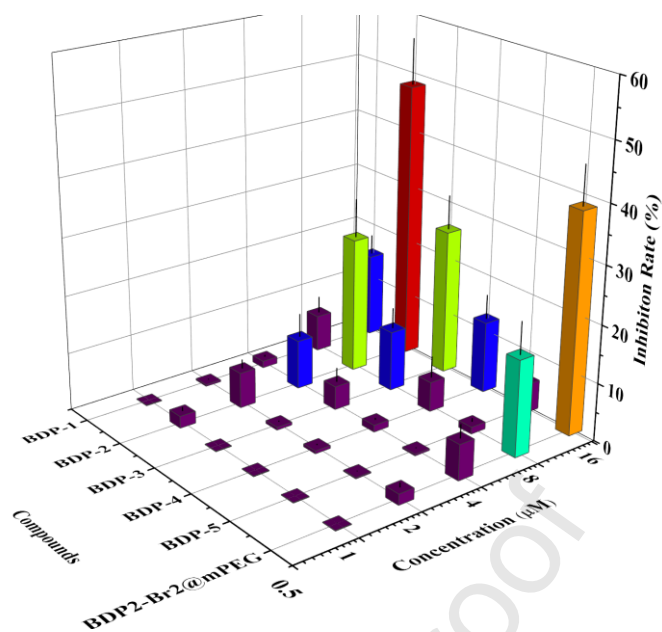


Fig. 5. Inhibition rates of five compounds (1 μM to 16 μM) and BDP2-Br₂@mPEG (6 $\mu\text{g}/\text{mL}$ to 96 $\mu\text{g}/\text{mL}$, its BDP2-Br₂ content: 1 μM to 16 μM) on *E. coli*. Data are expressed as the mean from three independent experiments.

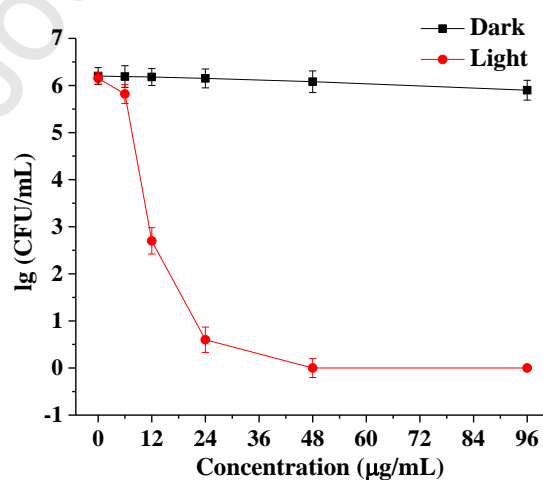


Fig. 6. Effects of increasing concentrations of BDP2-Br₂@mPEG on the photodynamic inactivation of *E. coli*. Light dose: 5 J/cm². Data are expressed as the means of three independent experiments ± SD.

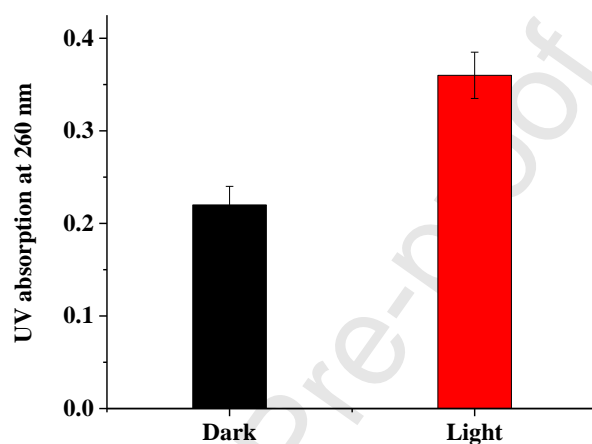


Fig. 7. Absorption at 260 nm of *E. coli* after incubated with BDP2-Br₂@mPEG under dark and LED light. The results are represented as mean ± SD (n = 3).

Table 1. Spectroscopic properties of BODIPYs at room temperature

Compunds	λ_{ex} (nm)	λ_{em} (nm)	$\Delta\lambda$ (nm)	$\epsilon \times 10^4$ (L·mol ⁻¹ ·cm ⁻¹)	Φ	τ (ns)
BDP-1	499	505	6	5.2	0.16	2.60
BDP-2	500	506	6	7.8	0.31	3.03
BDP-3	499	505	6	6.6	0.31	3.93
BDP-4	499	504	5	7.1	0.30	3.57
BDP-5	499	504	5	7.8	0.30	3.83
BDP2-Br ₂	526	535	9	7.6	0.18	3.68
BDP2-Br ₂ @mPEG	531	549	18	1.9	0.15	3.43

Note: $\Delta\lambda = \lambda_{em} - \lambda_{ex}$

Credit Author Statement

Jian Shao: Conceptualization, Methodology, Data Analysis, Writing and Original draft preparation. Pu-Zhen Huang: Synthesis. Qiu-Yun Chen: Supervision, Conceptualization, Writing Reviewing and Editing. Qing-Lin Zheng: Writing Reviewing and Editing.

Declaration of interests

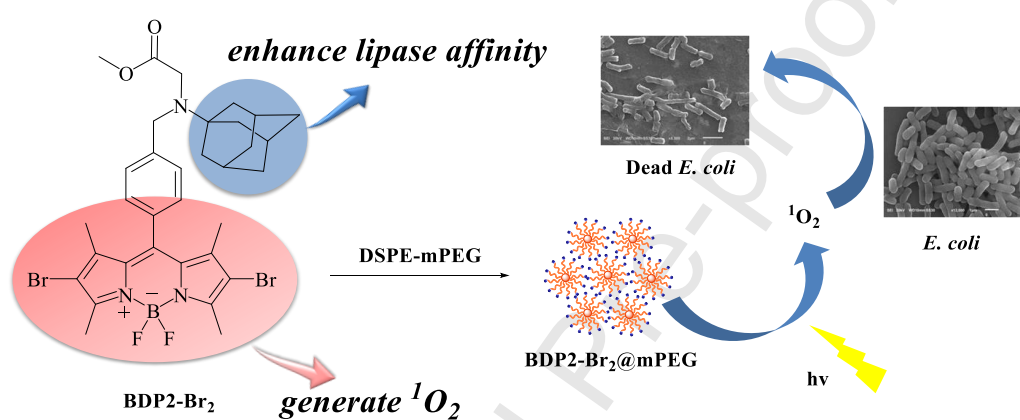
The authors declare that they have no known competing financial interests or personal relationships that could have appeared to influence the work reported in this paper.

The authors declare the following financial interests/personal relationships which may be considered as potential competing interests:

Graphical abstract

Nano adamantane-conjugated BODIPY for lipase affinity and light driven antibacterial

Jian Shao, Pu-Zhen Huang, Qiu-Yun Chen*, Qing-Lin Zheng



Highlights

- The spectroscopic features of five BODIPY derivatives were reported.
- Adamantane-conjugated BODIPY (BDP-2) exhibits high lipase affinity.
- Nano-dye was found to be photodriven antibacterial agent.

Journal Pre-proof

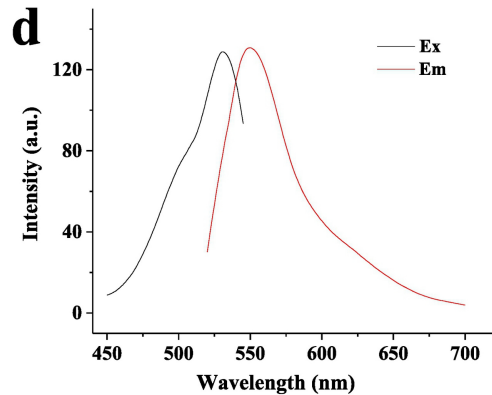
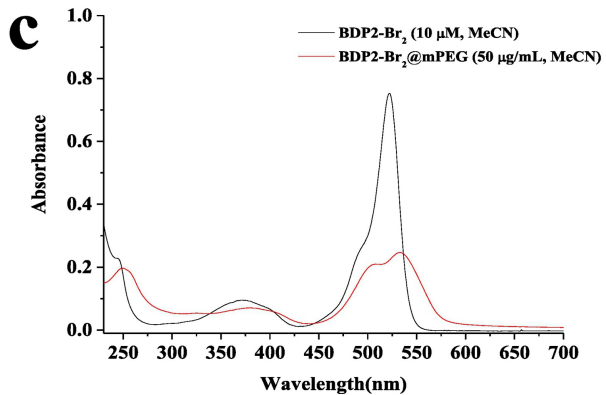
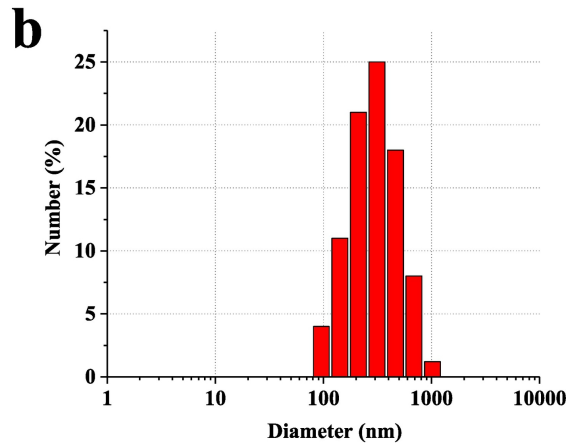
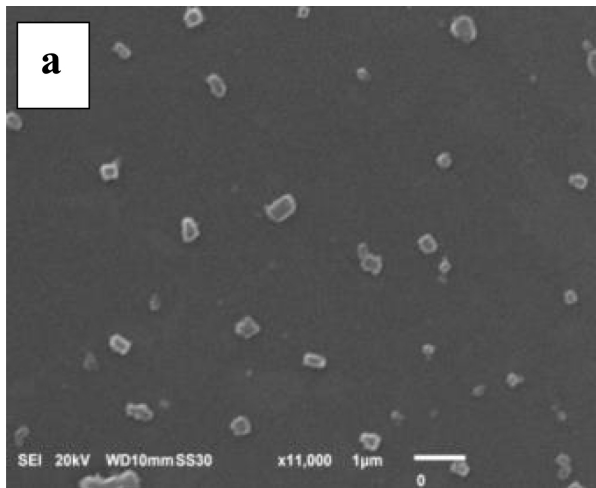


Figure 1

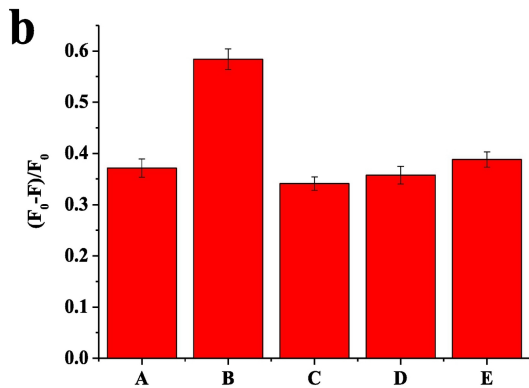
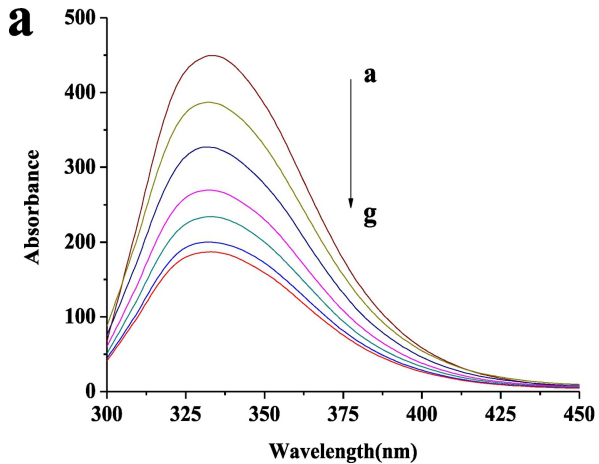


Figure 2

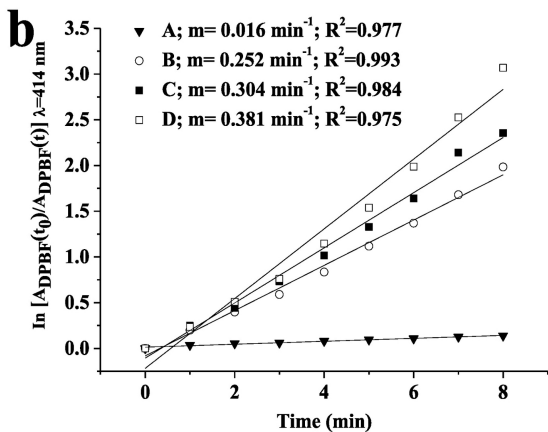
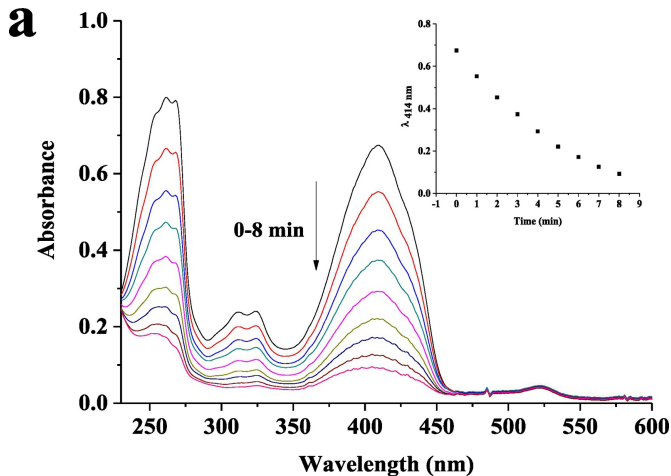


Figure 3

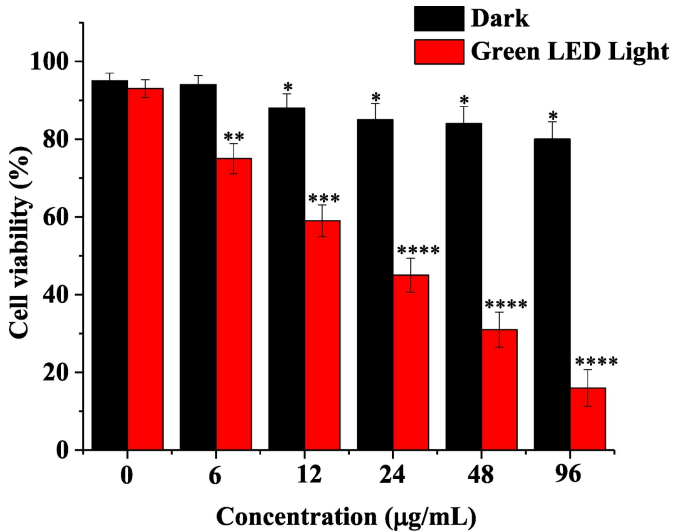


Figure 4

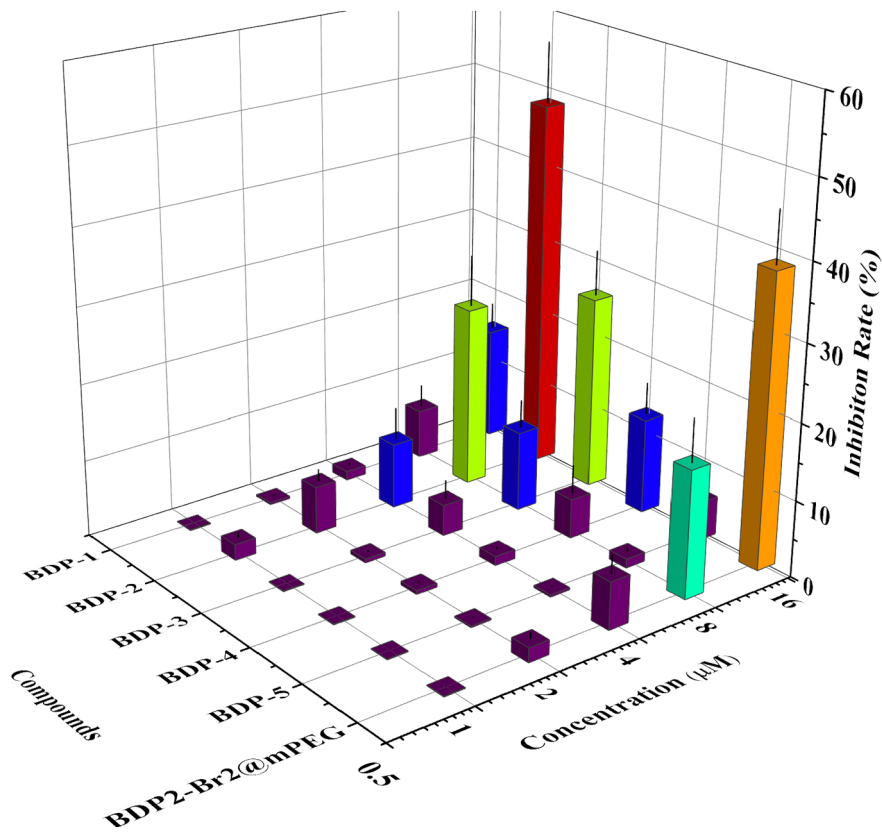


Figure 5

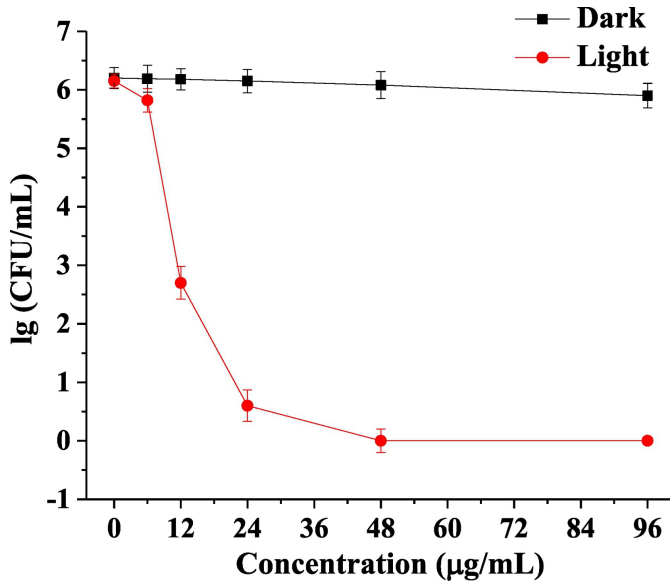


Figure 6

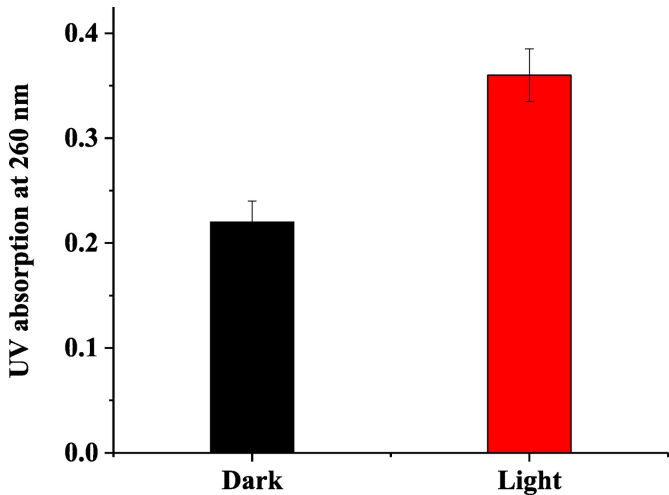


Figure 7